ADVANCED MATERIALS
www.advmat.de
www.MaterialsViews.com

COMMUNICATION

Charge-Carrier Dynamics and Mobilities in Formamidinium Lead Mixed-Halide Perovskites

*Waqaas Rehman, Rebecca L. Milot, Giles E. Eperon, Christian Wehrenfennig, Jessica L. Boland, Henry J. Snaith, Michael B. Johnston, and Laura M. Herz**

Recent years have seen the emergence of a promising new generation of hybrid organic–inorganic perovskite absorbers for highly efficient photovoltaic devices.[1–4] Materials with the perovskite crystal structure follow the general stoichiometry AMX_3. For the organic–inorganic perovskites studied so far, A is an organic cation, M is a metal cation such as Pb^{2+} or Sn^{2+}, and X_3 comprises one or more types of halide anions.[5] Early reports on perovskite absorbers in working photovoltaic devices demonstrated mesoporous metal-oxide liquid-electrolyte sensitized solar cells, which reached power conversion efficiencies (PCE) of a few percent.[6] Research soon moved toward more stable all-solid-state devices based on a range of different architectures incorporating hybrid interfaces. One concept emulates solid-state dye-sensitized solar cells (DSC), using the perovskite material as an absorber infiltrated into an electron-extracting mesoporous metal-oxide layer.[7] Alternatively, a meso-superstructured configuration incorporating an insulating mesoporous Al_2O_3 scaffold was demonstrated, which resulted in landmark PCEs of over 12%.[2,8] Finally, several fabrication methods have been developed for planar-heterojunction architectures[1,9] including a one-step spin-coating method from solution precursors,[7,10,11] a two-step sequential method,[3] and vapor-phase deposition in a vacuum chamber[1] which have accompanied a phenomenal increase of PCEs. The highest certified PCE of hybrid organic–inorganic perovskite solar cells (PSC) has reached 20.1% to date,[12–14] with methylammonium (MA) lead tri-iodide ($CH_3NH_3PbI_3$) and formamidinium (FA) lead tri-iodide ($HC(NH_2)_2PbI_3$) or mixtures thereof being the most frequently investigated perovskite absorbers. The outstanding performance of PSCs has been attributed to unique photophysical and material properties that are well suited for solar cell applications. In addition to high optical absorption coefficients of around 10^5 cm^{-1} in the visible range[15,16] and high charge-carrier mobilities, bimolecular charge-carrier recombination rates defy the Langevin limit for kinetic recombination by at least four orders of magnitude.[17,18] $MAPbI_3$ also appears to exhibit only shallow trap-levels and although the grain boundaries have recently been shown to induce nonradiative decay,[19] regions only a few tens of nm away from the grain boundaries appear to be unaffected.[20,21] Furthermore, low Urbach energies, which are extracted from near band edge optical absorption measurements and serve as a benchmark for crystalline phase disorder, indicate low disorder and sharp band edges for lead tri-halide perovskites (15–23 meV).[22,23] All of these properties contribute to high open-circuit voltages, long charge-carrier lifetimes, and micrometer diffusion lengths, which are crucial for planar-heterojunction photovoltaics.[1,24] Nonetheless, these parameters are also expected to depend on the influence of crystallization condition on perovskite morphology in fabricated films.[25]

A distinct benefit of organic–inorganic perovskite materials (e.g., over silicon) is that their bandgap can be tuned relatively easily with chemical composition, allowing attractive coloration and multijunction or tandem cell designs. For example, changing the metal cation at the M site from Pb^{2+} to the less toxic Sn^{2+} to form $CH_3NH_3SnI_3$ shifts the optical bandgap from 1.55 to 1.3 eV into the range of the "ideal" single-junction solar cell bandgap between 1.1 and 1.4 eV.[26,27] However, stability issues arising from the oxidation of tin have so far prevented widespread use. Alternatively, tuning the size of the A site cation has been proven to change optical and electronic properties of the perovskite and to significantly influence solar cell performance.[28] Replacing MA in $MAPbI_3$ by the larger cation formamidinium $HC(NH_2)_2^+$ (FA) was found to decrease the bandgap from 1.57 to 1.48 eV,[29–31] yield long photoluminescence (PL) lifetimes, high PCEs,[28] and lower recombination and device hysteresis.[32] Highest PCEs of 20.1% have been reported[12–14] to date for solar cells based on $FAPbI_3$ making this an attractive system to explore. In addition, the gradual replacement of the MA cation by FA through the film was shown to create a mixed cation-lead-iodide PSC allowing for energetic gradients.[33] However, mixing of the halide component in the perovskite offers the finest tuning of the optical properties of the perovskite film. Here, the mixed organic lead iodide/bromide system has recently gained strong interest for application in PSCs.[11,28] By changing the ratio between bromide and iodide (at the X site anion), the bandgap can be tailored between 1.55 eV ($MAPbI_3$) and 2.3 eV ($MAPbBr_3$), which results in the coverage of much of the visible spectrum and paves the way for the development of tandem solar cells.[11] In addition to $MAPb(Br_yI_{1-y})_3$, its formamidinium relative $FAPb(Br_yI_{1-y})_3$ has been explored.[28] Most fractional mixtures of $FAPb(Br_yI_{1-y})_3$ were found to be crystalline, with the exception of the region between $y = 0.3$ and

W. Rehman, Dr. R. L. Milot, G. E. Eperon, Dr. C. Wehrenfennig, J. L. Boland, Prof. H. J. Snaith, Prof. M. B. Johnston, Prof. L. M. Herz
Clarendon Laboratory
Oxford University
Parks Road, OX1 3PU Oxford, UK
E-mail: laura.herz@physics.ox.ac.uk

DOI: 10.1002/adma.201502969

$y = 0.5$ where the crystal structure changed, resulting in an amorphous region.[23,28] A number of studies exploring the characteristics of solar cells based on the $MAPbI_3$ to $MAPbBr_3$ material system have been performed.[34] However, given the importance of this heterogeneous material system, little is known about the dynamics of photoexcited charge-carriers and their mobilities as a function of iodide/bromide content. A deeper understanding of these properties is now essential for further improvement of photovoltaic devices based on these highly tunable materials.

Here we present a key analysis of the charge-carrier dynamics including recombination rate constants and mobilities across the range of compositions in the mixed-halide lead perovskite system $FAPb(Br_yI_{1-y})_3$. We demonstrate that bimolecular and Auger recombination rate constants directly correlate with the Br/I fraction and are insensitive to phase stability. With an increasing Br/I ratio, charge recombination rate constants increase by up to an order of magnitude, with bimolecular recombination however remaining significantly below the Langevin limit. Because of their lack of correlation with material morphology, we propose that these are intrinsic charge recombination mechanisms that are directly linked with changes in electronic structure induced, e.g., by modifications of the frontier orbitals upon halide substitution. Charge-carrier mobilities, on the other hand, exhibit a strong correlation with phase disorder. For the trihalide systems, $FAPbBr_3$ and $FAPbI_3$, we establish effective charge-carrier mobilities of (14 ± 2) cm^2 V^{-1} s^{-1} and (27 ± 2) cm^2 V^{-1} s^{-1}. For the intermediate mixed-halide materials, charge-carrier mobilities fall in correlation with increasing phase disorder, as evidenced by a rise in energetic broadening and trap-induced recombination mechanisms.

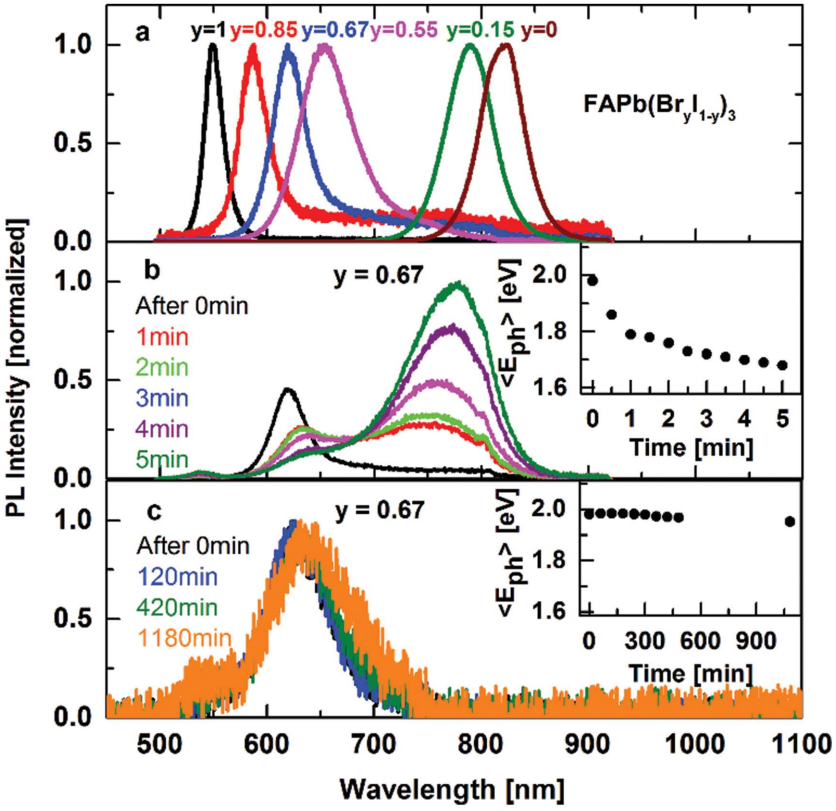

Figure 1. a) Steady-state photoluminescence (PL) spectra of thin films of $FAPb(Br_yI_{1-y})_3$ perovskite with varying halide composition y, recorded immediately following excitation at 400 nm at a fluence of 0.1 μJ cm^{-2} (7.2 W cm^{-2}) under vacuum. The PL spectra have been normalized to the peak emission. b) PL spectra of a $FAPb(Br_{0.67}I_{0.33})_3$ film over the course of 5 min of continuous illumination following excitation at 400 nm with an intensity of 7.2 W cm^{-2} (fluence of 0.1 μJ cm^{-2}, pulse duration 100 fs, repetition rate 80 MHz). Inset: Change of average photon energy $\langle E_{ph} \rangle$ as a function of illumination time. c) In situ PL spectra for a $FAPb(Br_{0.67}I_{0.33})_3$ film over the course of 1180 min of continuous illumination following excitation at 400 nm with an intensity of 15 mW cm^{-2} (fluence of 13.5 μJ cm^{-2}, pulse duration 40 fs, repetition rate 1.1 kHz). Spectra were collected in situ with a fiber-optic collection system under experimental conditions matching those used for time-resolved THz photoconductivity data shown in Figure 2. PL spectra have been normalized to the peak emission intensity. Inset: Change of the average photon energy $\langle E_{ph} \rangle$ as a function of time.

The $FAPb(Br_yI_{1-y})_3$ films were formed by spin-coating mixtures of 0.55 M $FAPbI_3$ and 0.55 M $FAPbBr_3$ in anhydrous *N,N*-dimethylformamide on warm substrates (85 °C) in a nitrogen-filled glovebox and annealing in air at 170 °C for 10 min. Prior to mixing the solutions, a small amount of acid was added to the $FAPbI_3$ and $FAPbBr_3$ solutions to enhance solubility of the precursors and allow ultrasmooth and pinhole-free film formation: 38 μL of hydroiodic acid (57% w/w) was added per 1 mL of the 0.55 M $FAPbI_3$ precursor solution, and 32 μL of hydrobromic acid (48% w/w) was added per 1 mL of the 0.55 M $FAPbBr_3$ precursor solution. This procedure gave very uniform pinhole-free layers of $FAPb(Br_yI_{1-y})_3$ with a thickness of ≈300–400 nm. A more detailed description can be found in the Supporting Information.

Figure 1a displays steady-state PL spectra for thin films of $FAPb(Br_yI_{1-y})_3$ with varying bromide content between $y = 0$ (100% iodide) and $y = 1$ (100% bromide). In agreement with previous reports,[9] the PL peak energy is found to tune continuously from 2.26 eV for $FAPbBr_3$ to 1.50 eV for $FAPbI_3$. Theoretical calculations show that the red shift upon moving from Br^- to I^- derives from the associated decrease of the electronegativity of the halogen atom.[35] Exchanging Br^- with I^- changes the nature of the halide frontier orbital contribution to the valence band from 4p to 5p, which decreases the bandgap energy.[36,37] The observed PL peak positions are consistent with the absorption onsets seen in absorbance spectra of the examined $FAPb(Br_yI_{1-y})_3$ films (see Figure S1, Supporting Information) confirming that the PL arises primarily from band-edge emission rather than from minority phases or trap states.

For $FAPb(Br_yI_{1-y})_3$ films with bromide content in the region $0.3 < y < 0.5$, the material quality appears significantly lowered, as apparent from the absence of significant PL emission and X-ray diffraction (XRD) data. While outside of this region, XRD shows sharp peaks arising from crystalline

perovskite,[28] the lack of such features in the intermediate region ($0.3 < y < 0.5$) suggests that the material becomes amorphous here (see Figure S6, Supporting Information) with "amorphous" implying that the crystalline order is on too short a length scale to be detectable in our XRD data. Such structural disorder can be understood in the context of a crystal structure change: while $FAPbI_3$ adopts the trigonal structure,[14,29] $FAPbBr_3$ is cubic at room temperature.[28] Variation of bromide content for this system has been shown to lead to a monotonic change in pseudocubic lattice parameter determined from XRD, apart from the transition region of $0.3 < y < 0.5$ between which the structure transfers from cubic to tetragonal and no well-defined crystal structure can be formed.[28] We therefore refer to this region as the "amorphous region" in our subsequent analysis.

In previous work, a reversible light-induced transformation of PL spectra for mixed iodide/bromide perovskites has been reported, which raised concerns regarding the photostability of these mixed halide materials.[38] Under constant illumination, bromide-rich $MAPb(Br_yI_{1-y})_3$ perovskite films were found to exhibit a new dominant peak at around 740 nm, i.e., red-shifted toward the emission spectrum of $MAPbI_3$.[38] It was proposed that photoexcitation may cause halide segregation into two crystalline phases: an iodide-rich minority domain and a bromide-rich majority domain.[38] This instability could be substantially detrimental for photovoltaic performance in solar cell devices since the expectation would be that the open-circuit voltage may then become limited by the energy of the lower bandgap phases. By contrast, other studies of PL emission from mixed-halide perovskite systems have not reported such light-induced shifts.[23,28] Here, we find that the intensity of the laser excitation spot plays a major role in producing these shifts. Figure 1b shows the PL emission of a $FAPb(Br_{0.67}I_{0.33})_3$ film (a composition on the Br side of the phase instability) when recorded for laser excitation with an intensity of 7.2 W cm^{-2} following 5 min of continuous illumination. Indeed, here, the phenomenon of halide migration-induced shifts is clearly corroborated. The original PL maximum at 620 nm almost completely shifts to a new dominant low-energy PL feature, which is recognizable at around 785 nm (1.58 eV). The luminescence intensity almost doubles with respect to the initial value, in accordance with higher PL emissivity of the iodide-rich phases. In addition, the enhancement of another small phase at around 540 nm (2.3 eV) is distinguishable. The inset of this figure presents the decrease of the average energy of emitted photons following pulsed laser excitation and shows a continuous decrease over time. Figure 1c, on the other hand, shows PL spectra for an identical $FAPb(Br_{0.67}I_{0.33})_3$ film under illumination at the same wavelength (400 nm) for 1180 min (20 h) with laser intensity of 15 mW cm^{-2}. These were collected with an in situ (fiber-based) spectrometer under conditions identical to those employed in the time-resolved THz photoconductivity measurement described below. With an excitation intensity 500 times lower, negligible shifts in PL maxima and average photon energy are observed (see Figure 1c), and no new low-energy PL features emerge during continuous laser excitation over the time-scale of 20 h. Additional measurements for films with other bromide fractions, which can be found in Figure S2 (Supporting Information), exhibit smaller shifts only for prolonged irradiation of films near the amorphous region ($y = 0.55$). While the primary aim of these measurements is to establish that the examined films do not phase-segregate or decompose during the time-resolved THz photoconductivity measurements described below, we note that photovoltaic devices are typically tested under AM1.5 conditions (1 kW m^{-2} = 100 mW cm^{-2}), which is closer to the light intensity of 15 mW cm^{-2} for which we do not observe significant PL peak shifts. These results may therefore explain why no instabilities in open-circuit voltages have so far been reported for mixed I^-/Br^- perovskite photovoltaic devices, and suggest that mixed-halide perovskites may yet be a usable route toward wider bandgap absorbers. They further highlight the need for more quantitative investigations into light-induced halide segregation in these mixed systems (e.g., dependences on light intensity, nonlinearities, heating, and morphology), which will ascertain the extent to which such effects are detrimental under photovoltaic device operating conditions.

With stability of materials under THz measurement conditions confirmed, we proceed by analyzing the charge-carrier recombination dynamics in the mixed-halide perovskites. Here we use ultrafast optical pump-THz probe spectroscopy as a time-resolved, contactless conductivity probe, which has been used previously to study charge-carrier recombination rate constants for other perovskite materials[17,18] (see the Supporting Information for full experimental details). The question as to which optically excited species may couple to the THz probe pulse, either excitons or free charge-carriers has been addressed several times in earlier reports.[17,18,39–42] We note that for $MAPbI_3$ the sole response to the THz conductivity probe has already been shown to be that of a free-charge carrier density, as inferred from the Drude shape of the conductivity spectra.[17,18] Here we also report highly similar Drude conductivity spectra for $FAPbBr_3$ (see the Supporting Information), which suggests that excitonic effects are negligible at room temperature for these mixed I/Br materials.

Figure 2 displays the THz photoconductivity transients following photoexcitation of films with four different compositions of $FAPb(Br_yI_{1-y})_3$ after photoexcitation at 400 nm with excitation fluences ranging from 8 to 65 μJ cm^{-2}. The transient conductivity originating from photoexcited charge carriers is probed by a THz radiation pulse at a precise time-delay with regard to the pump pulse. The data shown in Figure 2 reveal a striking correlation between the photoconductivity decay dynamics and bromide content. When the bromide fraction y is increased from $FAPbI_3$ ($y = 0$, Figure 2a) to the lighter-halide perovskite, $FAPbBr_3$ ($y = 1$, Figure 2d), the initial decay components of the transients gradually become faster. This suggests that upon change from neat-iodide to the neat-bromide perovskite film, higher order recombination effects increase.

The decline in photoconductivity with increasing time after excitation is primarily the result of charge-carrier recombination, which is expected to depend on the charge carrier-density and therefore laser excitation fluence.[17,18] For high charge-carrier densities, there will be an enhanced contribution from higher-order recombination mechanisms, such as second-order electron–hole (bimolecular) recombination as well as third-order Auger recombination, in which energy and momentum are transferred to a third charge-carrier.[18] Taking such effects

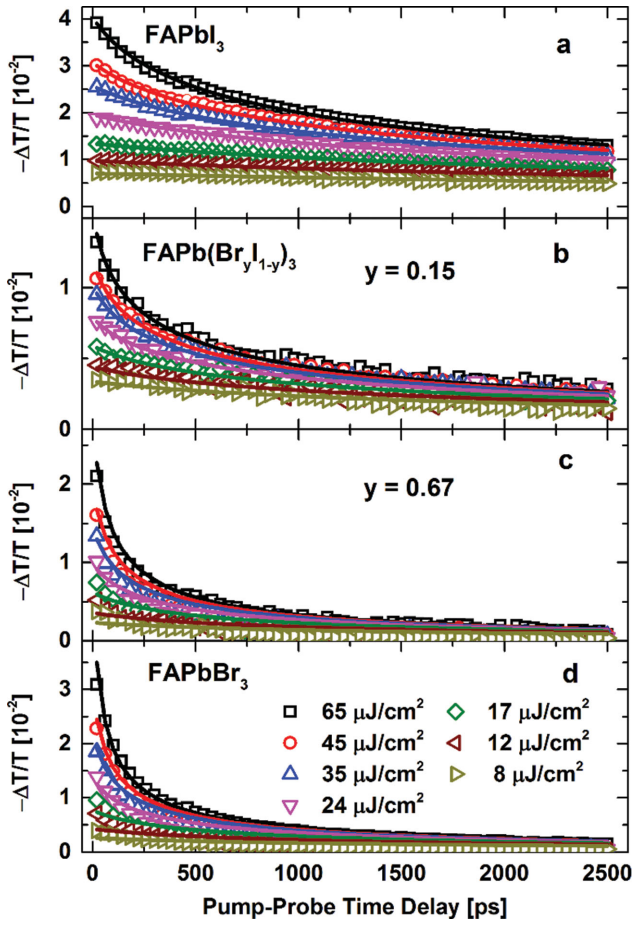

Figure 2. THz photoconductivity transients for thin films of $FAPb(Br_yI_{1-y})_3$ with a) $y = 0$, b) $y = 0.15$, c) $y = 0.67$, and d) $y = 1$, for excitation fluences between 8 and 65 μJ cm^{-2} at 400 nm wavelength. The symbols represent data points, and the solid lines are fits as described in the text.

into account, the associated recombination rate constants can be derived from fits to data of solutions to Equation (1):

$$\frac{dn(t)}{dt} = -k_3 n^3 - k_2 n^2 - k_1 n \quad (1)$$

where $n(t)$ is the free charge-carrier density, k_3 is the Auger recombination rate constant, k_2 is the bimolecular recombination rate constant, and k_1 is the monomolecular recombination rate, which may arise from charge trapping. Since the measured relative change in THz electric field transmission ($\Delta T/T$) is proportional to the photoinduced conductivity and thereby to the free charge-carrier density,[43] fitting the above rate equation to the transients allows the extraction of recombination rate constants (see the Supporting Information for details). Fitting was performed globally across all fluences, and the monomolecular decay rate constant k_1 was fixed to a value determined using time-resolved PL measurement at very low laser excitation densities for which higher-order recombination effects are negligible (see Supporting Information, Figure S3). However, we note that since the monomolecular lifetime k_1^{-1} is significantly larger than the observation window of 2.5 ns for which THz data were taken, the exact value of k_1 has little influence on the fits.

Figure 3 demonstrates that both the bimolecular (k_2) and Auger recombination rates (k_3) increase monotonically with increasing bromide content and are an order of magnitude lower for $FAPbI_3$ compared to the lighter-halide $FAPbBr_3$. These results are notable because they suggest a clear link between these intrinsic electron–hole recombination rate

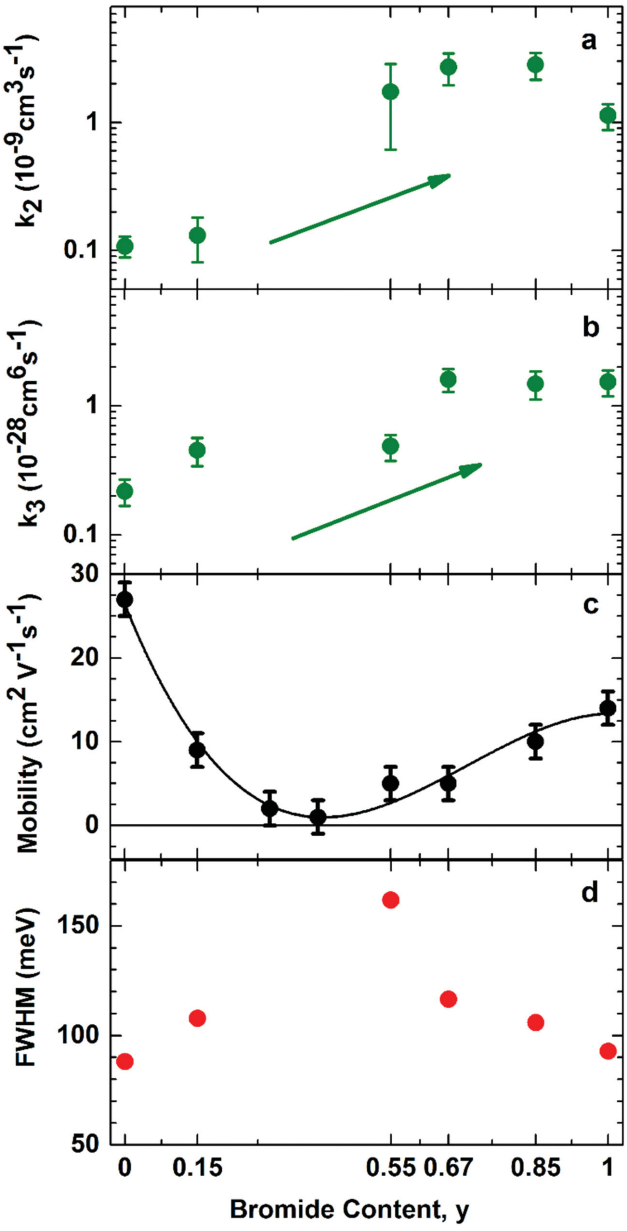

Figure 3. a) Bimolecular and b) Auger-recombination rate constants, k_2 and k_3, for varying bromide content y in thin films of $FAPb(Br_yI_{1-y})_3$ perovskite. The constants were extracted from fits to THz photoconductivity transients; values are also listed in Table S1 (Supporting Information). c) Effective charge-carrier mobilities of mixed-halide $FAPb(Br_yI_{1-y})_3$ perovskite films of varying bromide content. The solid line is a guide to the eye. d) Full width at half maximum (FWHM) of the PL emission peak versus bromide content.

constants and the composition and therefore electronic structure of the material. As discussed above, the material crystallinity is markedly lower toward the central region of $0.3 < \gamma < 0.5$, however, the bimolecular and Auger recombination rates appear relatively insensitive to this, changing instead monotonically with γ. As we show below, the situation is very different for the charge-carrier mobility and trap-related recombination rate, which are instead found to be strongly linked with material quality or crystallinity. However, bimolecular and Auger recombination do not show features near the central instability region, suggesting instead a correlation with fundamental electronic properties of the system. A gradual change in the intrinsic recombination parameters with bromide fraction may be expected for a number of reasons. First, the substitution of iodide with bromide changes the nature of the valence-band maximum, which has strong contributions from hybridizations of the atomic frontier p-orbitals of the halide[37] that may affect spontaneous bimolecular electron–hole recombination rates. In addition, the bimolecular recombination rates for hybrid metal-halide perovskites are suppressed well below the values predicted by Langevin theory, for which spatial segregation of electron–hole pairs across the metal-halide bond has been proposed as one possible origin.[17,18] We find similarly supressed Langevin ratios here across the whole $FAPb(Br_\gamma I_{1-\gamma})_3$ system (see Table S1, Supporting Information). Changes in halide composition may affect such spatial segregation and in turn tune the bimolecular recombination rates. For Auger recombination, rate constants generally depend strongly on the electronic band structure of the semiconductor because of the need for overall momentum and energy conservation involving the many-body process.[44] For the $FAPb(Br_\gamma I_{1-\gamma})_3$ system, a gradually decreasing pseudocubic lattice parameter has been reported with increasing bromide fraction[28] in agreement with a continuous change in electronic band structure; however, the exact correlation between Auger recombination and crystal structure is likely to be complex. Our investigations open up new possibilities for linking optoelectronic properties of these promising materials with calculations that may eventually allow materials design from first principles.

Charge-carrier mobilities also play a significant role in the performance of photovoltaic devices, affecting charge extraction to electrodes. We determined effective charge-carrier mobilities $\phi\mu$ for the mixed-halide $FAPb(Br_\gamma I_{1-\gamma})_3$ films from the photoconductivity onset value at zero pump-probe delay and with knowledge of the initially absorbed photon density and other optical parameters as further described in the Supporting Information. Although we derive effective charge-carrier mobilities as lower bounds of the actual mobility, we assume that the photon-to-free-charge conversion ratio ϕ is close to unity because of the observed Drude-like photoconductivity spectra, as discussed above.

Figure 3c displays the extracted charge-carrier mobility values as a function of bromide content. For $FAPbI_3$ ($\gamma = 0$), a value of (27 ± 2) cm^2 V^{-1} s^{-1} is found, similar to values previously determined for solution-processed meso-superstructured $MAPbI_3$ films[18] and vapor-deposited solid $MAPb(I_{1-x}Cl_x)_3$ films.[17] Interestingly, $FAPbBr_3$ ($\gamma = 1$) also shows a remarkably high mobility value of (14 ± 2) cm^2 V^{-1} s^{-1}, only lower by a factor of 2 than that for the iodide-only material. All of the examined mixed-halide materials, however, exhibit charge-carrier mobilities below these two limits. Unlike the bimolecular and Auger recombination kinetics discussed above, the obtained charge mobilities exhibit a clear correlation with increasing electronic disorder. For the amorphous intermediate-region films ($0.3 < \gamma < 0.5$), charge mobilities exhibit a significant drop decreasing down to (2 ± 2) cm^2 V^{-1} s^{-1} for $\gamma = 0.3$ and (1 ± 2) cm^2 V^{-1} s^{-1} for $\gamma = 0.4$ films. The full width at half maximum (FWHM) of the PL emission peaks from $MAPb(Br_\gamma I_{1-\gamma})_3$ films has recently been shown to be a reliable measure for phase stability, correlating directly with the Urbach energy.[23] Figure 3d shows the FWHM extracted from the PL peaks shown in Figure 1a for the $FAPb(Br_\gamma I_{1-\gamma})_3$ films investigated here. The PL FWHM shows clear correlation with the extracted charge-carrier mobility values, providing a direct link between the presence of disorder and a lowering in charge mobility. The neat tri-halide perovskite films display the lowest FWHM, in accordance with very low crystalline phase disorder and sharp band edges for these films.[23] In addition, we find that the mono-molecular recombination rate k_1 extracted from PL decay transients at low excitation fluence (see the Supporting Information) also exhibits a link with energetic disorder, although this may be superimposed on a general trend of increasing k_1 with increasing bromide content. Increasing disorder is likely to enhance such trap-induced monomolecular recombination, while changes in band structure may lead to modifications in relative trap energies, explaining the observed trends. Therefore, while single-halide lead perovskites show highly favorable charge-carrier lifetimes and transport, mixed-halide lead perovskites would benefit from newly devised routes toward manufacturing films with improved compositional homogeneity and therefore enhanced electronic order. Recent observations of strongly improved optoelectronic properties for $MAPbX_3$ ($X = Br^-$, I^-) single crystals grown by vapor-assisted crystallization demonstrate that decreasing disorder is a crucial aim for thin-film device applications.[45]

From the measured charge-carrier recombination constants and mobilities, we are able to extract charge-carrier diffusion lengths as a function of charge-carrier density (see Figure S5, Supporting Information), which are important figures of merit particularly for the use of these materials in planar-heterojunction device architectures. At a charge-carrier density of $n \approx 10^{15}$ cm^{-3} which is typical during photovoltaic device operation, we find that the charge carrier diffusion length exceeds 1 μm for the parameter space $0 < \gamma < 0.15$ and $\gamma = 1$, with the tri-iodide $FAPbI_3$ exhibiting the highest diffusion length of 3.1 μm and the tri-bromide $FAPbBr_3$ a value of 1.3 μm, lowered by the lower charge-carrier mobility and higher charge-carrier recombination rates. For these materials, charge-carrier diffusion lengths clearly exceed the optical absorption depth (typically about a few hundred nm across the visible), in good agreement with the successful demonstration of efficient planar-heterojunction photovoltaic cells for this range of γ.[28] For the mixed-halide materials within the amorphous region, we find charge-carrier diffusion lengths in the range of 500–700 nanometers at $n \approx 10^{15}$ cm^{-3}, which is still respectable but may start to reduce charge-carrier collection efficiencies and maximum attainable open-circuit voltages in planar-heterojunction devices. However, our results suggest that only relatively modest improvements in disorder and trap density are required in order to

make these Br-rich materials suitable for planar heterojunction device architectures.

We note that for elevated charge-carrier densities (>10^{16} cm^{-3}), diffusion lengths gradually decline, as bi-molecular recombination starts to play a role (see Figure S5, Supporting Information). Such scenarios may be of relevance for solar concentrator applications or in a charge-accumulation regime. However, relative trends across the $FAPb(Br_yI_{1-y})_3$ system are maintained, because of the strong correlation between structural disorder and the charge-carrier mobility. In addition, we stress that the charge-carrier diffusion lengths derived from such high-frequency THz measurements represent values that would be attributable to local domains with relatively unobstructed charge percolation pathways. Charge-carrier diffusion across a full film thickness may well encounter domain or crystal boundaries that act as additional barriers. Liang et al. have recently determined a charge-carrier diffusion length of ≈160 nm for $MAPb(I_{0.8}Br_{0.2})_3$ from diffusion induced PL quenching,[46] while Kedem et al. found 360 nm for $MAPbBr_3$(Cl) using cross-sectional electron-beam-induced current measurements.[47] These values are lower than those we establish for matching bromide fraction here, which may be partly caused by differences in composition (MA instead of FA) or processing, but may also partly derive from the long-range charge diffusion methods employed by these groups.

In this study we have presented key findings on the parameters governing charge-carrier dynamics and charge-carrier mobilities in a mixed-halide lead perovskite system. We find that the bimolecular and Auger recombination rate constants in $FAPb(Br_yI_{1-y})_3$ strongly correlate with the relative Br content y, which suggests an inherent link with electronic structure and halide frontier orbital composition. For $FAPbI_3$, both recombination rate constants, k_2 and k_3, are found to be an order of magnitude lower compared to the lighter-halide $FAPbBr_3$ film. Such links may allow for predictive correlations to be established between desired charge-recombination properties and material composition. Unlike the recombination rate constants, charge-carrier mobilities across the mixed Br^-/I^- system exhibit a striking dependence on crystalline phase disorder. For $FAPbBr_3$ and $FAPbI_3$ films we determine mobilities of (14 ± 2) cm^2 V^{-1} s^{-1} and (27 ± 2) cm^2 V^{-1} s^{-1}, respectively, whereas values for the mixed Br/I halide materials are lower than these two limits, and in comparison very low (<2 cm^2 V^{-1} s^{-1}) for the amorphous region between $y = 0.3$ and $y = 0.5$. As a result, both iodide-rich and neat-bromide materials exhibit charge-carrier diffusion lengths exceeding 1 µm, however, this drops to values of the order of a half a micrometer for the bromide-rich mixed systems. These findings suggest that lowering the energetic disorder in mixed-halide perovskites would significantly improve charge-carrier transport, allowing effective incorporation in planar-heterojunction tandem solar cell devices with high short-circuit currents, open-circuit voltages, and PCEs.

Supporting Information

Supporting Information is available from the Wiley Online Library or from the author.

Acknowledgements

The authors gratefully acknowledge funding from the Engineering and Physical Sciences Research Council (EPSRC). W.R. thanks the Hans-Böckler-Foundation for support through a doctoral scholarship. G.E.E. is supported by a CASE studentship from the EPSRC and Oxford Photovoltaics Ltd via the Nanotechnology KTN.

Received: June 19, 2015
Revised: July 29, 2015
Published online: September 24, 2015

[1] M. Liu, M. B. Johnston, H. J. Snaith, *Nature* **2013**, *501*, 395.
[2] M. M. Lee, J. Teuscher, T. Miyasaka, T. N. Murakami, H. J. Snaith, *Science* **2012**, *338*, 643.
[3] J. Burschka, N. Pellet, S. Moon, R. Humphry-Baker, P. Gao, M. K. Nazeeruddin, M. Grätzel, *Nature* **2013**, *499*, 316.
[4] I. Chung, B. Lee, J. He, R. P. Chang, M. G. Kanatzidis, *Nature* **2012**, *485*, 486.
[5] B. Wang, X. Xiao, T. Chen, *Nanoscale* **2014**, *6*, 12287.
[6] A. Kojima, K. Teshima, Y. Shirai, T. Miyasaka, *J. Am. Chem. Soc.* **2009**, *131*, 6050.
[7] H. Kim, C. Lee, J. Im, K. Lee, T. Moehl, A. Marchioro, S. Moon, R. Humphry-Baker, J. Yum, J. E. Moser, M. Grätzel, N.-G. Park, *Sci. Rep.* **2012**, *2*, 591.
[8] J. M. Ball, M. M. Lee, A. Hey, H. J. Snaith, *Energy Environ. Sci.* **2013**, *6*, 1739.
[9] O. Malinkiewicz, A. Yella, Y. H. Lee, G. M. Espallargas, M. Graetzel, M. K. Nazeeruddin, H. J. Bolink, *Nat. Photonics* **2014**, *8*, 128.
[10] J. H. Heo, S. H. Im, J. H. Noh, T. N. Mandal, C. Lim, J. A. Chang, Y. H. Lee, H. Kim, A. Sarkar, M. K. Nazeeruddin, *Nat. Photonics* **2013**, *7*, 486.
[11] J. H. Noh, S. H. Im, J. H. Heo, T. N. Mandal, S. I. Seok, *Nano Lett.* **2013**, *13*, 1764.
[12] H. Zhou, Q. Chen, G. Li, S. Luo, T. B. Song, H. S. Duan, Z. Hong, J. You, Y. Liu, Y. Yang, *Science* **2014**, *345*, 542.
[13] J. Im, I. Jang, N. Pellet, M. Grätzel, N. Park, *Nat. Nanotechnol.* **2014**, *9*, 927.
[14] W. S. Yang, J. H. Noh, N. J. Jeon, Y. C. Kim, S. Ryu, J. Seo, S. I. Seok, *Science* **2015**, *348*, 1234.
[15] H. J. Snaith, *J. Phys. Chem. Lett.* **2013**, *4*, 3623.
[16] M. A. Green, A. Ho-Baillie, H. J. Snaith, *Nat. Photonics* **2014**, *8*, 506.
[17] C. Wehrenfennig, M. Liu, H. J. Snaith, M. B. Johnston, L. M. Herz, *Energy Environ. Sci.* **2014**, *7*, 2269.
[18] C. Wehrenfennig, G. E. Eperon, M. B. Johnston, H. J. Snaith, L. M. Herz, *Adv. Mater.* **2014**, *26*, 1584.
[19] D. W. deQuilettes, S. M. Vorpahl, S. D. Stranks, H. Nagaoka, G. E. Eperon, M. E. Ziffer, H. J. Snaith, D. S. Ginger, *Science* **2015**, *348*, 683.
[20] W. Yin, T. Shi, Y. Yan, *Adv. Mater.* **2014**, *26*, 4653.
[21] E. Edri, S. Kirmayer, A. Henning, S. Mukhopadhyay, K. Gartsman, Y. Rosenwaks, G. Hodes, D. Cahen, *Nano Lett.* **2014**, *14*, 1000.
[22] S. De Wolf, J. Holovsky, S. Moon, P. Löper, B. Niesen, M. Ledinsky, F. Haug, J. Yum, C. Ballif, *J. Phys. Chem. Lett.* **2014**, *5*, 1035.
[23] A. Sadhanala, F. Deschler, T. H. Thomas, S. E. Dutton, K. C. Goedel, F. C. Hanusch, M. L. Lai, U. Steiner, T. Bein, P. Docampo, *J. Phys. Chem. Lett.* **2014**, *5*, 2501.
[24] S. D. Stranks, G. E. Eperon, G. Grancini, C. Menelaou, M. J. Alcocer, T. Leijtens, L. M. Herz, A. Petrozza, H. J. Snaith, *Science* **2013**, *342*, 341.
[25] T. Du, N. Wang, H. Chen, H. Lin, H. He, *ACS Appl. Mater. Interfaces.* **2015**, *7*, 3382.

[26] F. Hao, C. C. Stoumpos, D. H. Cao, R. P. Chang, M. G. Kanatzidis, *Nat. Photonics* **2014**, *8*, 489.
[27] N. K. Noel, S. D. Stranks, A. Abate, C. Wehrenfennig, S. Guarnera, A. Haghighirad, A. Sadhanala, G. E. Eperon, S. K. Pathak, M. B. Johnston, *Energy Environ. Sci.* **2014**, *7*, 3061.
[28] G. E. Eperon, S. D. Stranks, C. Menelaou, M. B. Johnston, L. M. Herz, H. J. Snaith, *Energy Environ. Sci.* **2014**, *7*, 982.
[29] C. C. Stoumpos, C. D. Malliakas, M. G. Kanatzidis, *Inorg. Chem.* **2013**, *52*, 9019.
[30] T. M. Koh, K. Fu, Y. Fang, S. Chen, T. Sum, N. Mathews, S. G. Mhaisalkar, P. P. Boix, T. Baikie, *J. Phys. Chem. C.* **2013**, *118*, 16458.
[31] A. Amat, E. Mosconi, E. Ronca, C. Quarti, P. Umari, M. K. Nazeeruddin, M. Grätzel, F. De Angelis, *Nano Lett.* **2014**, *14*, 3608.
[32] R. S. Sanchez, V. Gonzalez-Pedro, J. Lee, N. Park, Y. S. Kang, I. Mora-Sero, J. Bisquert, *J. Phys. Chem. Lett.* **2014**, *5*, 2357.
[33] N. Pellet, P. Gao, G. Gregori, T. Yang, M. K. Nazeeruddin, J. Maier, M. Grätzel, *Angew. Chem. Int. Ed.* **2014**, *53*, 3151.
[34] S. A. Kulkarni, T. Baikie, P. P. Boix, N. Yantara, N. Mathews, S. Mhaisalkar, *J. Mater. Chem. A.* **2014**, *2*, 9221.
[35] P. Gao, M. Grätzel, M. K. Nazeeruddin, *Energy Environ. Sci.* **2014**, *7*, 2448.
[36] A. Walsh, *J. Phys. Chem. C* **2015**, *119*, 5755.
[37] E. Mosconi, A. Amat, M. K. Nazeeruddin, M. Grätzel, F. De Angelis, *J. Phys. Chem. C* **2013**, *117*, 13902.
[38] E. T. Hoke, D. J. Slotcavage, E. R. Dohner, A. R. Bowring, H. I. Karunadasa, M. D. McGehee, *Chem. Sci.* **2015**, *6*, 613.
[39] M. Hirasawa, T. Ishihara, T. Goto, K. Uchida, N. Miura, *Phys. B* **1994**, *201*, 427.
[40] K. Tanaka, T. Takahashi, T. Ban, T. Kondo, K. Uchida, N. Miura, *Solid State Commun.* **2003**, *127*, 619.
[41] S. Sun, T. Salim, N. Mathews, M. Duchamp, C. Boothroyd, G. Xing, T. C. Sum, Y. M. Lam, *Energy Environ. Sci.* **2014**, *7*, 399.
[42] V. D'Innocenzo, G. Grancini, M. J. Alcocer, A. R. S. Kandada, S. D. Stranks, M. M. Lee, G. Lanzani, H. J. Snaith, A. Petrozza, *Nat. Commun.* **2014**, *5*, 3586.
[43] H. Nienhuys, V. Sundström, *Phys. Rev. B* **2005**, *71*, 235110.
[44] A. Haug, *J. Phys. C: Solid State Phys.* **1983**, *16*, 4159.
[45] D. Shi, V. Adinolfi, R. Comin, M. Yuan, E. Alarousu, A. Buin, Y. Chen, S. Hoogland, A. Rothenberger, K. Katsiev, Y. Losovyj, X. Zhang, P. A. Dowben, O. F. Mohammed, E. H. Sargent, O. M. Bakr, *Science* **2015**, *347*, 519.
[46] P. Liang, C. Chueh, X. Xin, F. Zuo, S. T. Williams, C. Liao, A. K. Jen, *Adv. Energy Mater.* **2015**, *5*, 1400960.
[47] N. Kedem, T. M. Brenner, M. Kulbak, N. Schaefer, S. Levcenko, I. Levine, D. Abou-Ras, G. Hodes, D. Cahen, *J. Phys. Chem. Lett.* **2015**, *6*, 2469.